

CFD based estimation of potential power saving for ships with fuel saving rudder-propeller device

Claus D. Simonsen, Christian Klimt Nielsen
FORCE Technology

Introduction

FORCE Technology, Grontmij | Carl Bro and Rolls Royce in Denmark have been involved in a joint project under DCMT (Danish Centre for Maritime Technology). Based on promising results obtained in [2] the goal of this project was to test and demonstrate the capabilities of RANS in connection with flow simulations for different rudder and propeller configurations. Focus was on a complete CFD model for hull, propeller and appendages, which can account for the mutual interaction between the components when the flow field is calculated.

In the present work different rudder-propeller configurations were evaluated behind a 180m bulk carrier in order to study how different configurations influence the ship performance for a given speed at the ships self-propulsion point. In order to check the performance of the CFD model, the calculated results are compared with experimental data measured in FORCE Technology's towing tank. All meshing and flow simulation are conducted with Star-CCM+ provided by CD-adapco.

The previous work from the project has been presented in [1]. In this work computations were done for the propeller in open water setup and for the hull with rudder in a calm water resistance setup. Propeller behind ship configurations were also considered, but it was not attempted to estimate the ships self-propulsion point, so instead the propeller revolutions were fixed at the experimental measured value during the simulation and the computed propeller thrust and torque were compared with the corresponding measured data. The agreement between computation and measurement was reasonable for the thrust and torque values, but when it came prediction of the change in required power between different rudder-propeller configurations at self-propulsion point larger differences were obtained. It was difficult to say exactly why, but since the power difference is based on very small changes in the propeller torque one has to be very careful when setting up the CFD model. A number of possible reasons for the variations were identified: 1) one could be small differences between the real model test propeller and the CAD based CFD propeller, 2) different meshing approach and distribution of cell refinement zones on and around the propeller and finally 3) using the

measured self propulsion point settings does not give self propulsion in the CFD model due to numerical errors, i.e. when the experimental RPMs are used the computed thrust does not balance the computed resistance and consequently the target relaxation force is not correct.

In the work presented below the three issues identified above were investigated to study the influence on the results.

Test case and CFD method

The goal of this task is to investigate how the CFD model can capture the influence on power when changing rudder-propeller configuration. For this purpose it is necessary to study the self propulsion case, since the different propellers must be running at self propulsion point to give the correct power for comparison between configurations. The study is carried out for the 180m Diamond 34 Bulk Carrier from Grontmij | Carl Bro, Figure 1. Two rudder-propeller configurations are considered: 1) is ship with original rudder and propeller and 2) is ship equipped with a PROMAS solution from Rolls Royce. The computations are done in model scale using a scale of 1:23.73. The main particulars and propeller data for the base configuration are shown in Table 1. Finally, one model speed condition was chosen for all configurations namely 1.479 m/s (14 knots full scale) corresponding to a Froude number of 0.173.

L_{pp}	[m]	7.449
B	[m]	1.264
T	[m]	0.411
S	[m ²]	15.533
C_B	[-]	0.80
D_p	[m]	0.236
Z	[no. of blades]	4
$P/D_{0.7}$	[-]	0.839

Table 1: Hull and propeller data.

The PROMAS geometry was fitted to the Diamond 34 by Rolls Royce. The design was based on basic

geometric information and wake field measurements previously done on the vessel [4]. In Figure 2, the original rudder propeller configuration is shown together with the PROMAS configuration. Compared to the “as built” configuration several differences are seen for the PROMAS configuration:

- The leading edge of the rudder is closer to the propeller
- The propeller geometry is different
- There is a rudder bulb on the PROMAS rudder plus a hub fairing



Figure 1: 180m bulk carrier.

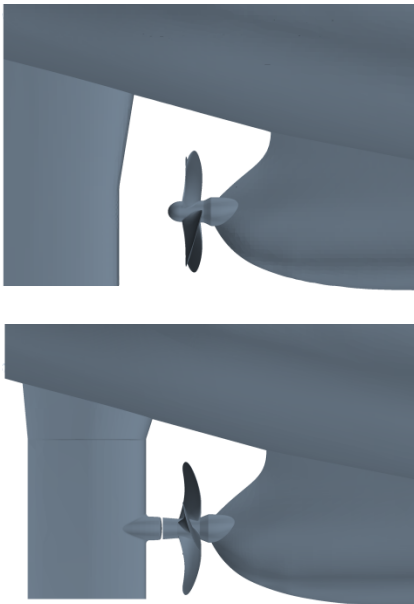


Figure 2: Upper: Original design (Base case). Lower: PROMAS design

Further, the rudder on the PROMAS comes with a weak asymmetry, since the leading edge is slightly twisted to meet the propeller swirl. The original rudder is straight and symmetric. The PROMAS propeller differs from the original one by having a smaller diameter and a smaller pitch ratio, Table 2.

D_p	[m]	0.228
Z	[no. of blades]	4
$P/D_{0.7}$	[-]	0.777

Table 2: Main propeller characteristics for the PROMAS propeller – model scale

The computations are performed with the Reynolds Averaged Navier-Stokes (RANS) solver StarCCM+ from CD-adapco. The code solves the RANS and continuity equations on integral form on a unstructured mesh by means of the finite volume technique. Both steady state and transient calculations are considered. For the steady state open-water calculations the temporal discretization is based on a first order Euler difference, while a second order difference is used for transient calculations with the rotating propeller. Spatial discretization is performed with second order schemes for both convective and viscous terms. The pressure and the velocities are coupled by means of the SIMPLE method. Closure of the Reynolds stress problem is achieved by means of the isotropic blended $k-\epsilon/k-\omega$ SST turbulence model with an all Y^+ wall treatment. The rotating propeller is treated in different ways depending on the propeller setup. For open water calculations the propeller inflow is uniform, so the moving reference frame approach is applied, i.e. the blade velocity is set on the propeller blades and centripetal effects are included in additional source terms in the momentum equations. For the propeller rotating behind the ship, a rigid body approach is applied. The free surface is modeled with the two phase volume of fluid technique (VOF). Further details about the code can be found in [3].

Simulation of open water configuration

The effort done to address the model issues listed in the introduction is described below. Concerning usage of similar grids, the considered propellers were re-gridded and improvement of the current meshes was attempted by changing meshing approach from trimmed meshes to polyhedral meshes. This type of mesh is assumed to give a better resolution of the geometry due to the shape of the polyhedral cells, particularly in the blade edge regions. In addition to this, the mesh topology and the overall cell size were also made as similar as possible on the considered propellers. Further, identical cell sizes and refinement zones were applied along the edges in order to resolve the flow features in a similar way. Figure 3 shows the improved meshes for two different propellers.

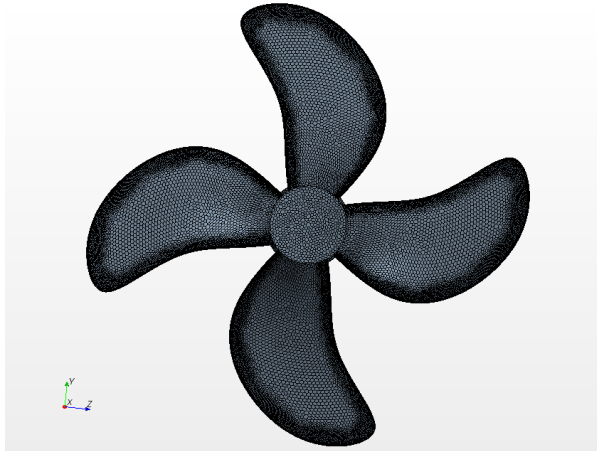
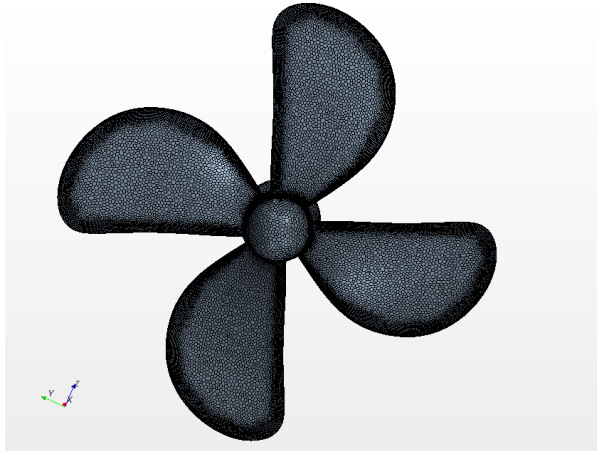


Figure 3: Improved polyhedral meshes. Upper: Original design (Base case). Lower: PROMAS design

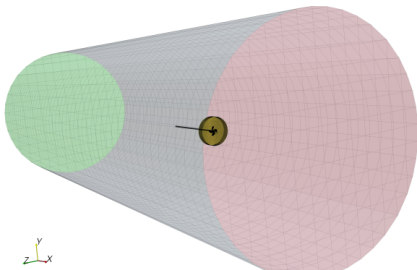


Figure 4: Computational grid for open water propeller.

Concerning the similarity between the CFD and model test propeller for the original propeller, it should be noted that the available CAD definition of the propeller was not in perfect condition near the blade edges, which made meshing a little complicated. To check the differences, a 3D scan of the original base case propeller was conducted in order to compare the available geometry of the CAD propeller and the model test propeller. In spite of small local differences, the comparison between the scanned image and the CAD model showed reasonable agreement.

After improving the meshes and scanning the propeller, new open water simulations were conducted for three different advance ratios. The propellers were set up in a large cylindrical domain, with a local smaller cylinder around it, *Figure 4*. The flow solver was run in steady mode and the rotation of the propeller was accounted for by means of the moving reference frame approach. This approach works fine in open water, where the propeller sees a completely uniform inflow field. Like in the experiment the computed thrust and torque on the propeller were converted into the dimensionless thrust coefficient K_T , torque coefficient K_Q and the open water efficiency η_0 . The advance ratio J and the three coefficients are defined as

$$J = \frac{U_a}{nD}$$

where U_a is the speed of advance, n is the propeller revolution rate and D is the propeller diameter.

The thrust coefficient K_T and torque coefficient K_Q are defined as

$$K_T = \frac{T}{\rho n^2 D^4} \quad K_Q = \frac{Q}{\rho n^2 D^5}$$

where T and Q are the measured thrust and torque, respectively. ρ is the density of water.

The propeller efficiency is defined as

$$\eta_0 = \frac{J}{2\pi} \frac{K_T}{K_Q}$$

J=0.3	CFD		EFD		Deviation in %	
	T	Q	T	Q	T	Q
Original	133.13	3.48	139.12	3.75	-4.3	-7.1
Original scanned	132.86	3.45	139.12	3.75	-4.5	-8.1
PROMAS	171.57	4.54	179.46	4.86	-4.4	-6.6

Table 3: Open-water results for $J=0.3$.

J=0.5	CFD		EFD		Deviation in %	
	T	Q	T	Q	T	Q
Original	83.73	2.43	85.36	2.59	-1.9	-6.1
Original scanned	84.49	2.42	85.36	2.59	-1.0	-6.6
PROMAS	119.17	3.48	123.79	3.74	-3.7	-7.0

Table 4: Open-water results for $J=0.5$.

J=0.7	CFD		EFD		Deviation in %	
	T	Q	T	Q	T	Q
Original	26.74	1.06	23.95	1.20	11.6	-11.8
Original scanned	28.21	1.09	23.95	1.20	17.8	-9.4
PROMAS	57.41	2.04	59.81	2.41	-4.0	-15.3

Table 5: Open-water results for $J=0.7$.

The results of the open-water computations with the new meshes are shown in *Table 3* to *Table 5*. As was found in previous work [2] reasonable agreement between measurement and computation is also found

here. The best agreement is found for the medium load propeller at $J=0.5$. It can be noted that except for the highest J value the CFD prediction seems to under predict the propeller thrust and torque. Concerning application of the scanned propeller compared to the CAD based propeller small changes are observed, but they are not radically changing the agreement between measurement and computation.

Simulation of self-propelled ship

In this case both hull and rudder are modeled with a trimmed mesh, which is a hexa-dominant polyhedral mesh. The hull-rudder grid is the same as used in [1]. The propeller is modeled with typical polyhedral cells as discussed above. The cylindrical propeller region used in the complete hull-propeller model is the exact same as the near-propeller mesh used for the open-water computations above. Since the propeller is running behind the ship, both sides of the hull are considered instead of exploiting the centre plane symmetry. The new grid is shown in Figure 5 and Figure 6. The near wall spacing of the grids on no-slip surfaces are in the range from $y^+ \approx 1$ to $y^+ \approx 30$.

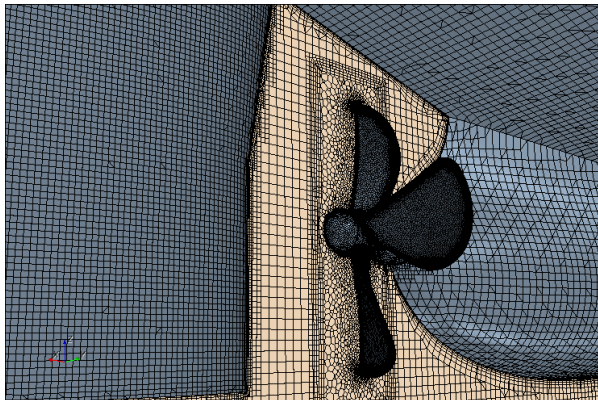


Figure 5: Computational grid on hull, rudder and original propeller.

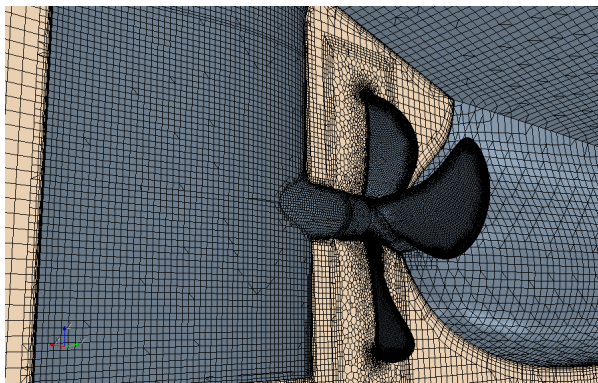


Figure 6: Computational grid on hull, rudder and PROMAS propeller.

In opposition to the work done in [1] and [2] where the number of propeller revolutions was taken from measurements, it is now predicted in order to find the propeller revolutions at the self-propulsion point. The applied approach is the same as used in the towing tank. This means that first the theoretical relaxation force, i.e. the additional target towing force is determined for the considered model speed. Afterwards two CFD simulations are conducted for two conditions with relaxation forces close to the target value. One is done propeller revolutions that give a too high relaxation force and the other is done with revolutions that give a too low relaxation force. With the two corresponding sets of relaxation forces and propeller revolutions, linear interpolation is performed in order to find the propeller revolutions that give the target value. The computations presented below are done for one model speed equal to 1.479 m/s. In the figures below, the pressure distribution is shown for suction and pressure sides of the propeller in the configuration with the original propeller and conventional rudder. The general flow features for the combined hull-propeller model were presented and discussed in [1]. A comparison between the features found in [1] and the present results shows that the change of propeller grid has not changed the overall picture of the flow field. This means that it can still be seen how the propeller is working harder (higher negative dynamic pressure on suction side) in areas where the surrounding fluid has to be accelerated the most, namely where the propeller blade passes the uppermost low speed region around the 12 o'clock position, Figure 7. The closer one gets the hull surface, the slower the fluid velocity will be, due to the presence of the hull boundary layer and the “shadow” from the skeg.

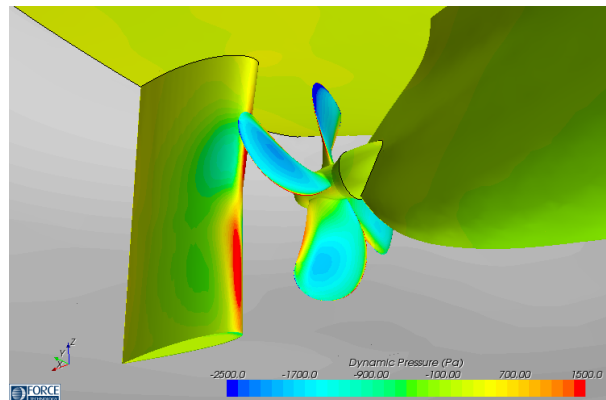


Figure 7: Starboard side, suction side

On the pressure side, Figure 8, the same effect is noticed – higher pressure as the propeller blade rotates through the low velocity zone in the upper part of the wake. Finally, the load on the blade also reflects the cross flow direction in the wake, i.e. the load reflects whether the blade moves downwards or upwards through the wake. More details on the flow features can be found in [1].

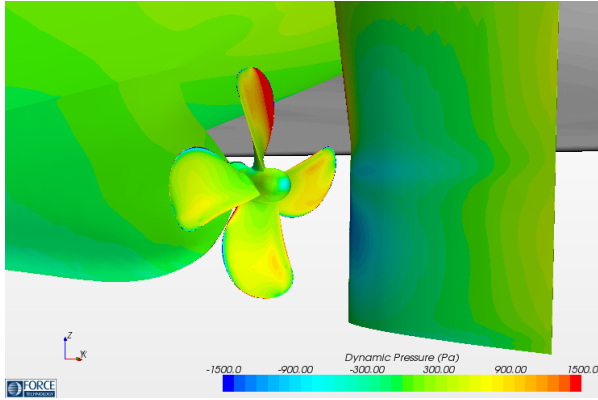


Figure 8: Port side, pressure side.

Moving to the integral quantities, focus will be on the results represented by towing force, propeller thrust and torque plus propeller revolutions for the original propeller and the PROMAS propeller. Table 6 and Table 7 show the results from four computations used for the CFD based self-propulsion prediction. The target towing force is 21.019N and the propeller RPM's were selected in order to give tow rope forces above and below the target value.

Point 1				
Speed	Thrust [N]	Torque [Nm]	RPM [rpm]	Rt [N]
1.479	45.885	1.350	564.546	19.000
Point 2				
Speed	Thrust [N]	Torque [Nm]	RPM [rpm]	Rt [N]
1.479	42.180	1.243	548.546	22.255

Table 6 Results used for prediction of self-propulsion point with original propeller

Point 1				
Speed	Thrust [N]	Torque [Nm]	RPM [rpm]	Rt [N]
1.479	45.618	1.290	558.005	19.241
Point 2				
Speed	Thrust [N]	Torque [Nm]	RPM [rpm]	Rt [N]
1.479	42.290	1.196	543.005	22.119

Table 7 Results used for prediction of self-propulsion point with PROMAS propeller

Self prop CFD:				
Speed	Thrust [N]	Torque [Nm]	RPM [rpm]	P [W]
1.479	43.59	1.28	554.62	74.55
Self prop EXP:				
Speed	Thrust [N]	Torque [Nm]	RPM [rpm]	P [W]
1.479	44.34	1.33	572.55	79.74
Difference in %:				
	Thrust	Torque	RPM	P [W]
	-1.70	-3.49	-3.13	-6.51

Table 8 Prediction of self-propulsion points with original propeller

Based on linear interpolation with respect to the towing force, the thrust, torque and RMPs corresponding to the target towing force are found. The values are shown in Table 8 and Table 9. From the tables it is seen that relatively good agreement between measurement, [4], [5] and computations is obtained. The computation generally seems to under predict the computed quantities for both the original and the PROMAS propeller.

Self prop CFD:				
Speed	Thrust [N]	Torque [Nm]	RPM [rpm]	P [W]
1.479	43.56	1.23	548.74	70.78
Self prop EXP:				
Speed	Thrust [N]	Torque [Nm]	RPM [rpm]	P [W]
1.479	44.07	1.32	558.01	77.33
Difference in %:				
	Thrust	Torque	RPM	P [W]
	-1.16	-6.92	-1.66	-8.46

Table 9 Prediction of self-propulsion points with PROMAS propeller

Concerning the power P at self propulsion it is computed based on the propeller torque calculated by

$$P = \frac{2 \pi Q \Omega_p}{60}$$

where Q is the torque, Ω_p is the propeller revolutions in rotations per minute. Based on the power values in Table 8 and Table 9 the reduction in required power when going from the original propeller to the PROMAS solution can be calculated. The results are shown in Table 10.

	CFD	EXP
% change in P	-5.06	-3.03

Table 10. Reduction of required P between original and PROMAS propeller. Predicted by CFD and EFD.

It is seen that the experiment predicts a reduction of 3% with the PROMAS propeller, while the CFD simulation gives a reduction of 5%. It seems that CFD is able to rank the PROMAS configuration compared to the original propeller, i.e. point out that the PROMAS solution is better. When it comes to quantification of the power saving CFD over predicts the saving, but taking the complexity of the flow problem and the uncertainties of both simulation and measurement the result looks promising and indicates a potential for RANS CFD to be used in connection with evaluation of fuel saving devices.

Concluding remarks

In the present work RANS CFD has been used to perform numerical open water, resistance and self-propulsion tests for a bulk carrier equipped with a conventional rudder-propeller configuration and a PROMAS configuration. Except for the rudder region, the hull grids are basically similar for all simulations. The propeller grids have been generated in a systematic way, so refinement zones, topology and mesh type are the same for both propellers. Finally, a check was made of the CAD based propeller geometry by comparison with a 3D scan of the physical model propeller.

The numerical open water test shows that thrust and torque values are predicted fairly well compared to measured data. Though, a tendency for under prediction of T and Q is noted for both propellers, except for high advance coefficients where CFD over predicts T for the PROMAS propeller. Comparison of data obtained with the original CAD geometry (which had quality issues) and the scanned geometry shows small deviations, but does not change the overall trends in the comparison with the measured data.

The self propulsion computations are run in order to predict the propeller revolutions at self propulsion and not as in previous work by taking the model tests values. The applied approach is similar to the one used for determination of the self-propulsion point in model testing, i.e. interpolation in relaxation force to obtain theoretical target value.

Focus in the present work is not on the flow field, since this was covered in previous work. However, a brief check of the flow field shows how the load on the propeller blade is influenced by the wake and evidently high pressure gradients are observed at both the leading and trailing edges. It can clearly be seen that the rotating propeller gives an asymmetric load distribution on the rudder. So the present model gives results in line with previous findings.

Regarding propeller forces and moments in the behind the ship condition it is seen that the CFD model can predict the thrust and torque within 1 to 7%. The thrust and torque are generally both under predicted for both the original propeller and the PROMAS propeller. Concerning the ability to predict the power saving between propeller configurations with CFD, the work shows that CFD is able to rank the PROMAS concept over the conventional rudder-propeller configuration, which was also done by the model test. When it comes to quantification of the power saving CFD over predicts the saving by saying 5% instead of the 3% obtained in the model test, but taking the complexity of the flow problem and the uncertainties of both simulation and measurement the result looks promising and indicates

the RANS CFD may be useful for evaluation of fuel saving devices in the future.

Future activities

As indicated above the application of CFD for evaluation of fuel saving devices looks promising, but to draw a firm conclusion, the tool needs to be applied on other devices and comparisons between computations and measurements need to be performed in order to carefully check how well the CFD tool works.

Acknowledgements

This research is sponsored in parts by The Danish Maritime Foundation through DCMT.

References

- [1] *Simonsen C. D. Nielsen, C., K. and Kishev, Z* "Using CFD for Simulation of Ships with Different Fuel Saving Rudder-Propeller Devices" *Numerical Towing Tank Symposium, Duisburg, Germany, 10-12 October 2010*
- [2] *Simonsen, C.D. and Carstens, R.,* "RANS simulation of the flow around a ship appended with rudder, ice fins and rotating propeller," *proceedings from NuTTS08, Brest France, 2008*
- [3] *StarCCM+ Users manual*
- [4] *FORCE Technology report no. 107-26802*
- [5] *FORCE Technology report no. 107-24345.08-1B*